 doi:10.20944/preprints202206.0290.v1

Article

Different Modes of Combustion Wave on a Lattice Burner

Vasily Novozhilov [a,*], Boris Lidskii [b] and Vladimir Posvyanskii [b]

[a] Victoria University, Melbourne, VIC 8001, Australia
[b] N.N. Semenov Federal Research Centre for Chemical Physics, Russian Academy of Sciences, 4 Kosygina St., Building 1, Russian Federation 119991
* Correspondence: vasily.novozhilov@vu.edu.au.

Abstract: Stabilization of planar premixed flame front on a lattice (porous) burner is considered. It is rigorously mathematically proved that there exist two different stabilization regimes: one with flame front located nearby the surface of the burner, and another with flame front located inside the lattice. These two regimes result in qualitatively different gas temperature profiles along the flow, that is monotonic and non-monotonic, respectively. Boundary between the two regimes is described in terms of dependence of the lattice solid material temperature on flow Peclet number. Likewise temperature profiles, such dependencies may be both monotonic and non-monotonic. Transition between the two types of dependencies is controlled by Arrhenius number. Conclusions of the study are supported by numerical analysis. They also compare favourably with available experimental data. Novelty of the present approach is fundamentally rigorous analytical analysis of the problem.

Keywords: premixed lattice burner; flame stabilization; analytical model

1. Introduction

Combustion waves are commonly emerge as a natural way of flame spread. Classical theory of combustion waves, covering laminar premixed flame propagation in pipes, and flame front propagation in solid reactive media is widely known [1-6].

There are other well-recognised types of combustion wave processes, for example, flame spread over surfaces of solid materials [7,8].

Investigation of combustion waves with homogeneous multi-phase heat exchange within the wave structure has been somewhat more recent. One type of such process is convective combustion where reacting gases interact with either combustible or inert matrix of porous material [9-14].

Another is standing combustion wave developing on a lattice (porous) burner (Figure 1). The latter device is of significant importance, both theoretically and practically.

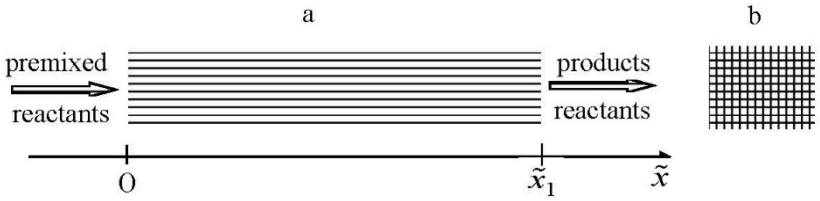

Figure 1. Schematic of the lattice burner considered. (a) side view (cross-section); (b) front (upstream) view.

Combustion process in porous burners has been studied extensively [15-29], using both experimental and numerical modelling methods, with respect to different burner configurations, combustion regimes and employed fuels (for example, biofuels). Recently Arutyunov *et al*. [30], using numerical methods, investigated nature of the upper limit of methane-air mixture combustion on a flat porous lattice. They demonstrated that position of the flame front, relative to the lattice surface, depends strongly on the heat exchange

Preprints (www.preprints.org) | NOT PEER-REVIEWED | Posted: 21 June 2022 doi:10.20944/preprints202206.0290.v1

rate between the gas and the solid lattice material. Within certain ranges of fuel preheating and injection rates unstable combustion regimes were observed, However, rigorous analytical studies of this combustion system have not been conducted.

The present paper investigates combustion wave structure on a lattice (that is on a laminar premixed porous burner). The study rigorously proves existence of the two distinctive combustion wave modes, with monotonic and non-monotonic temperature profiles, respectively.

The existence of double-mode wave structure, rigorously proven in the present paper, agrees qualitatively with experimental evidence, as discussed below.

2. Mathematical formulation

Assuming one-dimensional flow structure and uniform material properties (of both the gas and the solid lattice), the following steady-state Heat Transfer Equation (HTE) is considered to model the combustion process

$$\tilde{\lambda}\frac{d^2\tilde{T}}{d\tilde{x}^2}-\tilde{\rho}\tilde{c}_p\tilde{u}\frac{d\tilde{T}}{d\tilde{x}}+\tilde{Q}\tilde{A}\tilde{C}^2\left(\tilde{T}-\tilde{T}_0\right)^{1/2}\exp\left(-\frac{\tilde{E}}{\tilde{R}\tilde{T}}\right)+\tilde{h}\tilde{S}\left(\tilde{T}_s-\tilde{T}\right)=0 \qquad (1)$$

$$\tilde{h}=\begin{cases}\tilde{h}_s>0;\ \tilde{x}\in\left[0,\tilde{x}_1\right]\\ 0;\ \tilde{x}\in\left(\tilde{x}_1,\infty\right]\end{cases}$$

Flow is directed from left to right, and the lattice occupies the region from 0 to $\tilde{x}_1$ (Figure 1).

The third term on the Left Hand Side (LHS) of equation (1) describes contribution from bimolecular reaction occurring in premixed stream. Concentrations of both reactants are assumed to be equal at all times, i.e. $\tilde{C}_1\left(\tilde{x}\right)=\tilde{C}_2\left(\tilde{x}\right)=\tilde{C}\left(\tilde{x}\right)$. The fourth term describes heat transfer process between the gas and the solid lattice, with the heat transfer coefficient being assumed constant.

Chemical reaction rate is written in the form which makes it vanish at the initial temperature $\tilde{T}_0$. This is a standard assumption in the combustion theory.

The kinetic equation is

$$-\tilde{u}\frac{d\tilde{C}}{d\tilde{x}}=\tilde{A}\tilde{C}^2\left(\tilde{T}-\tilde{T}_0\right)^{1/2}\exp\left(-\frac{\tilde{E}}{\tilde{R}\tilde{T}}\right) \qquad (2)$$

Further simplification which is being made is that variable concentration $\tilde{C}$ is replaced on the Right Hand Side (RHS) of (2) by its initial value $\tilde{C}\equiv\tilde{C}_0\equiv const$. This is reasonable in the view of much stronger dependence on reaction rate on temperature, compared to dependence on reactant concentrations.

Simplified kinetic equation takes the form

$$-\tilde{u}\frac{d\tilde{C}}{d\tilde{x}}=\tilde{A}\tilde{C}_0^2\left(\tilde{T}-\tilde{T}_0\right)^{1/2}\exp\left(-\frac{\tilde{E}}{\tilde{R}\tilde{T}}\right) \qquad (3)$$

The following non-dimensional (scaling) variables are introduced

Preprints (www.preprints.org) | NOT PEER-REVIEWED | Posted: 21 June 2022 doi:10.20944/preprints202206.0290.v1

$$\xi = \frac{\tilde{x}}{\tilde{x}_1}; \qquad \theta = \frac{\tilde{T} - \tilde{T}_0}{\left(\tilde{R}\tilde{T}_0^2 / \tilde{E}\right)}; \qquad Pe = \frac{\tilde{x}_1 \tilde{u}}{\tilde{\kappa}}; \qquad C = \frac{\tilde{C}}{\tilde{C}_0}$$

$$A = \tilde{Q}\tilde{A}\tilde{C}_0^2 \frac{\tilde{x}_1^2}{\tilde{\lambda}} \left(\frac{\tilde{R}\tilde{T}_0^2}{\tilde{E}}\right)^{-1/2} \cdot \exp\left(-\frac{\tilde{E}}{\tilde{R}\tilde{T}_0}\right); \qquad h = \frac{\tilde{h}\tilde{S}\tilde{x}_1^2}{\tilde{\lambda}} \qquad (4)$$

$$g = \frac{\tilde{x}_1^2}{\tilde{\kappa}} \tilde{A}\tilde{C}_0 \left(\frac{\tilde{R}\tilde{T}_0^2}{\tilde{E}}\right)^{1/2} \cdot \exp\left(-\frac{\tilde{E}}{\tilde{R}\tilde{T}_0}\right)$$

The problem formulation becomes

$$\frac{d^2\theta}{d\xi^2} - Pe\frac{d\theta}{d\xi} + Af\left(\theta\right)C^2\left(\theta\right)H\left(C\right) + h\left(\theta_s - \theta\right) = 0$$

$$\frac{dC}{d\xi} = -\frac{g}{Pe} f\left(\theta\right)H\left(C\right) \qquad (5)$$

$$f\left(\theta\right) = \sqrt{\theta}\exp\left(\frac{\theta}{1 + Ar\theta}\right)$$

$$0 \le \xi \le L$$

$$\theta_s > 0, \qquad h = \begin{cases} h_s > 0; \ \xi \in [0,1] \\ 0; \ \xi \in (1, L] \end{cases}$$

with the boundary conditions

$$\theta\left(0\right) = \theta_0, \qquad C\left(0\right) = 1, \qquad \frac{d\theta}{d\xi}\left(L\right) = 0 \qquad (6)$$

where $L > 0$ is arbitrarily large number.

Here, for convenience of mathematical proofs, we assume that the temperature at the left boundary is slightly different from zero, i.e. $\theta_0 > 0$ is arbitrarily small positive number.

3. Results and discussion

3.1. Types of solutions

First of all, we demonstrate existence of solutions of the set of equations (5) with the boundary conditions (6).

This follows from the few Lemmas proved below.

Let us consider the set of equations (5) with the boundary conditions

Preprints (www.preprints.org) | NOT PEER-REVIEWED | Posted: 21 June 2022 doi:10.20944/preprints202206.0290.v1

$$\theta(0)=\theta_0, \qquad C(0)=1, \qquad \frac{d\theta}{d\xi}(0)=p \tag{7}$$

where p may assume any real value.

Define ξ_k in the following way: $\xi_k = L$ if $\theta(\xi)\neq 0$ on $[0,L)$; otherwise ξ_k is such that $\theta(\xi_k)=0$ and $\theta(\xi)\neq 0$ on $[0,\xi_k)$.

Lemma 1.

ξ_k, $\theta(\xi_k)$ and $\frac{d\theta}{d\xi}(\xi_k)$ are continuous functions of p.

Proof.

The statement is correct for $\xi_k \leq 1$ since solution of the Cauchy problem depends continuously on initial conditions.

If $\xi_k > 1$ then $\theta(1)$ and $\frac{d\theta}{d\xi}(1)$ depend on p continuously. Therefore, ξ_k, $\theta(\xi_k)$ and $\frac{d\theta}{d\xi}(\xi_k)$ are also continuous functions of p.

□

Lemma 2.

For any p_s there exists p such that for some ξ_s $\theta(\xi_s)=\theta_s$ and $\frac{d\theta}{d\xi}(\xi_s) > p_s$.

Proof.

Re-write the set of equations (5) in the form

$$\frac{d^2\theta}{d\xi^2} - Pe\frac{d\theta}{d\xi} - A\frac{Pe}{g}\frac{dC}{d\xi}C^2(\theta)H(C) + h(\theta_s-\theta)=0 \tag{8}$$

$$\frac{dC}{d\xi} = -\frac{g}{Pe}f(\theta)H(C)$$

and integrate the first equation on $[0,\xi]$.

Preprints (www.preprints.org) | NOT PEER-REVIEWED | Posted: 21 June 2022 doi:10.20944/preprints202206.0290.v1

We get

$$\frac{d\theta}{d\xi}(\xi) = p + Pe\left(\theta(\xi) - \theta_0\right) - \frac{APe}{3g}\left(1 - C^3 H(C)\right) - \int_0^{\xi} h_s\left(\theta_s - \theta\right) d\xi \tag{9}$$

Therefore,

$$\frac{d\theta}{d\xi}(\xi) > p - \frac{APe}{3g} - \xi h_s \theta_s \tag{10}$$

Let us chose now

$$p > p_s + \frac{APe}{3g} + \frac{h_s \theta_s^2}{p_s} \tag{11}$$

Then, for $\xi \in \left[0, \frac{\theta_s}{p_s}\right]$,

$$\frac{d\theta}{d\xi}(\xi) > p_s \;\; ; \;\; \theta\left(\frac{\theta_s}{p_s}\right) > \theta_s \tag{12}$$

□

Lemma 3.

$\theta(\xi)$ increase monotonically if $p_s > \frac{APe}{3g}$.

Proof.

Integrating (8) on $\left[\xi_s, \xi\right]$ we get

$$\frac{d\theta}{d\xi}(\xi) = p_s + Pe\left(\theta(\xi) - \theta_s\right) - \frac{APe}{3g}\left(1 - C^3 H(C)\right) + \int_{\xi_s}^{\xi} h_s\left(\theta(\alpha) - \theta_s\right) d\alpha \tag{13}$$

□

Lemma 4.

There exists p_0 such that $\xi_k = L$ and $\theta(\xi_k) = 0$.

Proof.

Let $q = \xi_k - L$ if $\xi_k < L$, and $q = \theta(\xi_k)$ if $\xi_k = L$. Then q is continuous function of p which assumes both positive and negative values.

□

Preprints (www.preprints.org) | NOT PEER-REVIEWED | Posted: 21 June 2022 doi:10.20944/preprints202206.0290.v1

THEOREM I (*Existence of solution*)

There exists a solution of the set of equations (5) with the boundary conditions (6).

Proof.

$\frac{d\theta}{d\xi}(L)$ is continuous function of p on $[p_0, +\infty)$. Since $\frac{d\theta}{d\xi}(L) \le 0$ at $p = p_0$, and there exists p such that $\frac{d\theta}{d\xi}(L) > 0$ then $\frac{d\theta}{d\xi}(L) = 0$ at some $p \in [p_0, +\infty)$.

□

In the following analysis of the set of equations (5) $\mu = \frac{A}{3g}$ will be assumed to be a large parameter.

Let us define ξ_0 in the following way:

$$C(\xi_0) = 0 \;;\; C(\xi) \neq 0 \text{ on } [0, \xi_0) \qquad (14)$$

The following 3 cases are possible

1) ξ_0 does not exist ($C(\xi) \neq 0$ on $[0, L)$)

2) $1 < \xi_0 \le L$

3) $0 < \xi_0 \le 1$

Consider first the case $1 < \xi_0 \le L$.

For $\xi_0 > 1$ the set (5) assumes the form

$$\frac{d^2\theta}{d\xi^2} - Pe\frac{d\theta}{d\xi} - 3\mu Pe\frac{dC}{d\xi}C^2(\theta)H(C) = 0$$

$$\frac{dC}{d\xi} = -\frac{g}{Pe} f(\theta) H(C) \qquad (15)$$

Lemma 5.

For $\xi \in [1, \xi_0]$ $\theta(\xi)$ does not decrease; for $\xi \in [\xi_0, L]$ $\theta(\xi) = \theta(\xi_0) = \theta^*$.

Proof.

Preprints (www.preprints.org) | NOT PEER-REVIEWED | Posted: 21 June 2022 doi:10.20944/preprints202206.0290.v1

This follows easily from (15) and the condition $\frac{d\theta}{d\xi}(L)=0$.

□

Let now $\theta(\xi_0)=\theta^*$. Integrating (15) we get

$$\frac{d\theta}{d\xi}-Pe\,\theta-\mu PeC^3(\xi)H(C)=-Pe\,\theta^* \tag{16}$$

Let now, for $0\le\hat{\xi}\le\xi_0$, $u(\hat{\xi})=\theta^*-\theta(\xi_0-\hat{\xi})$; $\hat{C}(\hat{\xi})=C(\xi_0-\hat{\xi})$.

The set of equations (15) takes the form

$$\frac{du}{d\hat{\xi}}+Pe\,u=\mu Pe\hat{C}^3$$

$$\frac{d\hat{C}}{d\hat{\xi}}=\frac{g}{Pe}f(\theta^*-u) \tag{17}$$

$$u(0)=\hat{C}(0)=0$$

It follows from (17) that $\frac{du}{d\hat{\xi}}<\mu Pe\hat{C}^3$.

Therefore

$$\mu Pe\frac{d\hat{C}}{d\hat{\xi}}\hat{C}^3>\frac{g}{Pe}\frac{du}{d\hat{\xi}}f(\theta^*-u) \tag{18}$$

Integrating (18) on $\left[0,\hat{\xi}\right]$ we obtain

$$\frac{\mu Pe}{4}\hat{C}^4>\frac{g}{Pe}\int_{\theta^*-u}^{\theta^*}f(\theta)d\theta \tag{19}$$

Let $\alpha=\left.\frac{d\ln f(\theta)}{d\theta}\right|_{\theta=\theta^*}$.

Preprints (www.preprints.org) | NOT PEER-REVIEWED | Posted: 21 June 2022 doi:10.20944/preprints202206.0290.v1

Lemma 6.

$$f(\theta) > \alpha \int_0^{\theta} f(w)\,dw \tag{20}$$

Proof.

Indeed, $\frac{d \ln f(\theta)}{d\theta} = \frac{1}{2\theta} + \frac{1}{(1+Ar\,\theta)^2}$ is monotonically decreasing function of θ. Therefore, for $w < \theta$ $\ln f(w) < \ln f(\theta) + \alpha(w-\theta)$, or $f(w) < f(\theta)\exp(\alpha(w-\theta))$. Integrating the later inequality, we prove Lemma 6.

□

Further, define the constant $\hat{C}_0$ by

$$\frac{\mu Pe}{4}\left(\hat{C}_0\right)^4 = \frac{g}{Pe}\int_0^{\theta^*} f(\theta)\,d\theta \tag{21}$$

Lemma 7.

$$\frac{d\hat{C}}{d\hat{\xi}} > \frac{\alpha\mu Pe}{4}\left(\left(\hat{C}_0\right)^4 - \hat{C}^4\right) \tag{22}$$

Proof.

It follows from Lemma 6 that

$$\frac{d\hat{C}}{d\hat{\xi}} > \frac{\alpha g}{Pe}\int_0^{\theta^*-u} f(w)\,dw = \frac{\alpha g}{Pe}\int_0^{\theta^*} f(w)\,dw - \frac{\alpha g}{Pe}\int_{\theta^*-u}^{\theta^*} f(w)\,dw \tag{23}$$

Since $\frac{\alpha g}{Pe}\int_0^{\theta^*} f(w)\,dw = \frac{\alpha\mu Pe}{4}\left(\hat{C}_0\right)^4$ and, according to (19) $\frac{\alpha\mu Pe}{4}\hat{C}^4 > \frac{\alpha g}{Pe}\int_{\theta^*-u}^{\theta^*} f(w)\,dw$, then Lemma 7 is proved.

Preprints (www.preprints.org) | NOT PEER-REVIEWED | Posted: 21 June 2022 doi:10.20944/preprints202206.0290.v1

□

Lemma 8.

$$\hat{C} > C_0\left(1-2\exp\left(\frac{\pi}{2}\right)\exp\left(-\alpha\mu PeC_0^3\hat{\xi}\right)\right) \tag{24}$$

Proof.

Consider the following equation

$$\frac{dy}{d\varsigma} = \kappa\left(\left(\hat{C}_0\right)^4 - y^4\right) \quad ; \quad y(0) = 0 \tag{25}$$

for $\varsigma \geq 0$, $y < \hat{C}_0$.

Its exact solution is

$$\kappa\varsigma = \frac{1}{4\left(\hat{C}_0\right)^3}\ln\left(\frac{\hat{C}_0 + y}{\hat{C}_0 - y}\right) + \frac{1}{2\left(\hat{C}_0\right)^3}arctg\left(\frac{y}{\hat{C}_0}\right) \tag{26}$$

Since $y < \hat{C}_0$ $arctg\left(\frac{y}{\hat{C}_0}\right) < \frac{\pi}{4}$ and we obtain

$$4\left(\hat{C}_0\right)^3\kappa\varsigma - \frac{\pi}{2} < \ln\left(\frac{\hat{C}_0 + y}{\hat{C}_0 - y}\right) \tag{27}$$

or

$$y > \hat{C}_0\left(1 - \frac{2}{1+\exp\left(4\left(\hat{C}_0\right)^3\kappa\varsigma - \frac{\pi}{2}\right)}\right) \tag{28}$$

Upon comparison with (22) Lemma 8 is proved.

□

Preprints (www.preprints.org) | NOT PEER-REVIEWED | Posted: 21 June 2022 doi:10.20944/preprints202206.0290.v1

We have actually shown that for $\alpha\mu \gg 1$ and $\xi_0 > 1$ (where $h \equiv 0$) solution of the set of equations

$$\frac{d^2\theta}{d\xi^2} - Pe\frac{d\theta}{d\xi} + \mu Pe\delta\left(\xi - \xi_0\right) + h\left(\theta_s - \theta\right) = 0$$

$$\theta\left(\xi_0\right) = \theta^*$$

$$\frac{\mu Pe}{4}C^4\left(1\right) = \frac{g}{Pe}\int_0^{\theta^*} f\left(w\right)dw \qquad (29)$$

$$\theta\left(0\right) = 0 \qquad \frac{d\theta}{d\xi}\left(L\right) = 0 \qquad \xi \in \left[1, L\right]$$

is a good approximation for solution of the set of equations (5) on the interval $\xi \in \left[1, L\right]$.

It may be shown by similar arguments that for $0 < \xi_0 < 1$ (where $h > 0$) solution of the set of equations (5) is also well approximated by the solution of the set of equations (29).

The requirements for μ given by the conditions $\alpha\mu \gg 1$ and the third of the conditions (29) enforces narrow reaction zone.

Analytical solution of the Boundary Value Problem (BVP) (29) is presented in the Appendix A.

This analytical solution delivers two different types of temperature profile, that is non-monotonic and monotonic. These occur, for example, for the sets of parameters shown in captions to Figures 2 and 3, respectively.

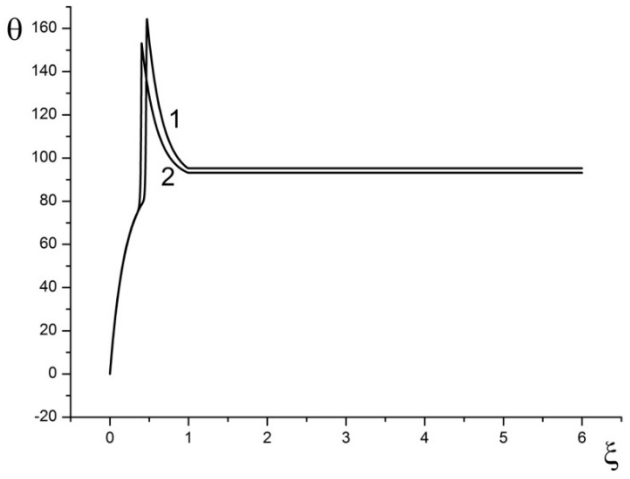

Figure 2. Non-monotonic solutions. 1 – approximate model (29); 2 – original model (5); Pe=135; A=2.75x10^{-18}; Ar=0.012; h_s=7.14x10^2; θ_s =90; g=1.0x10^{-20}; μ =91.67; ξ_0 =0.41.

Preprints (www.preprints.org) | NOT PEER-REVIEWED | Posted: 21 June 2022 doi:10.20944/preprints202206.0290.v1

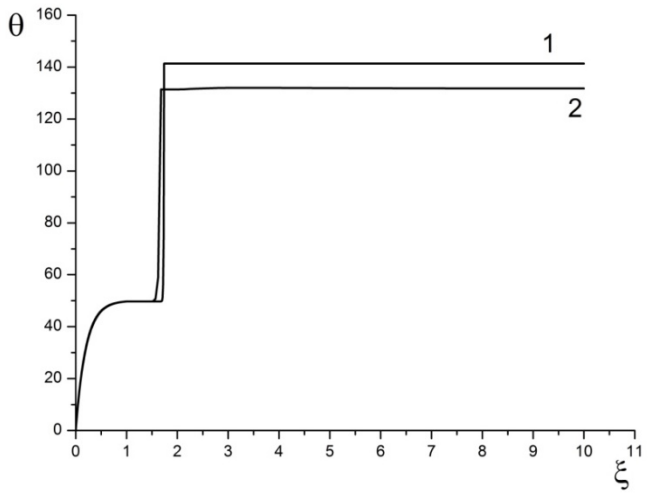

Figure 3. Monotonic solutions. 1 – approximate model (29); 2 – original model (5); Pe=135; A=2.75x10^{-18}; Ar=0.012; h_s=7.14x10^2; θ_s =50; g=1.0x10^{-20}; μ =91.67; ξ_0 =1.74.

Since the Lemmas 5 - 8 prove approximation of the problem (5) by the problem (29), and the two types of solutions can be demonstrated for (29), then the following Theorem below, the major result of the paper, has been proved.

THEOREM II (*Existence of the two types of solutions*)

The set of equations (5,6) admits two types of temperature profile solutions: monotonic and non-monotonic.

3.2 Numerical results

The Boundary Value Problem (5,6) may be solved numerically. False time transient method is used with the following numerical scheme

$$\frac{\theta_k^{n+1}-\theta_k^n}{\tau}=\frac{2}{\left(h_k+h_{k+1}\right)}\left[\frac{\theta_{k+1}^{n+1}-\theta_k^{n+1}}{h_{k+1}}-\frac{\theta_k^{n+1}-\theta_{k-1}^{n+1}}{h_k}\right]-Pe\frac{\left(\theta_k^{n+1}-\theta_{k-1}^{n+1}\right)}{h_k}+$$

$$+Af\left(\theta_k^n\right)\left(C_k^n\right)^2+h_s\left(\theta_s-\theta_k^{n+1}\right)$$

(30)

$$C_k^n=\left(1-\frac{g}{Pe}\int_0^{\xi_k} f\left(\theta^n(s)\right)ds\right)H\left(C_k^n\right)$$

Iterations are performed until steady-state solution is achieved, with certain *a'priori* specified accuracy.

Preprints (www.preprints.org) | NOT PEER-REVIEWED | Posted: 21 June 2022 doi:10.20944/preprints202206.0290.v1

Based on existing data [31,32] physically meaningful ranges of the problem parameters are identified as follows:

$$Pe \in [4, 280],$$

$$A \in \left[4.7 \times 10^{-29}, 4.7 \times 10^{-12}\right],$$

$$Ar \in \left[1.2 \times 10^{-2}, 2.0 \times 10^{-2}\right],$$

$$g \in \left[9.7 \times 10^{-29}, 9.84 \times 10^{-12}\right],$$

$$\mu \in [75.0, 208.0],$$

$$\theta_s \in [50.0, 705.0],$$

$$h_s \in \left[7.14 \times 10^{2}, 1.14 \times 10^{3}\right]$$

It should be remembered that besides the above restrictions for the parameters A, g and μ the relation $\mu = \dfrac{A}{3g}$ must always hold.

Numerical solutions plotted in Figures 2,3 confirm good approximation provided by (29) to the problem (5), as has been proved earlier in the Section 3.1.

Analytical solutions of the approximating problem (29) (Appendix A) show that this problem has non-monotonic solutions for $0 < \xi_0 < 1$ and monotonic for $\xi_0 > 1$.

It is instructive to identify, in the parameter space, the regions corresponding to the two types of solutions.

For this purpose, let us introduce the "critical curve", defined by the condition $\xi_0 = 1$ since the latter separates the two different types of solutions. From the equation (5)

$$1 - C(\xi) = \frac{g}{Pe} \int_0^{\xi} f\left(\theta(s)\right) ds \qquad (31)$$

Therefore, due to definition (14), the requirement $\xi_0 = 1$ translates into the following relationship between the governing parameters θ_s and Pe (with the parameter g being considered fixed)

$$\frac{g}{Pe} \int_0^{1} f\left(\theta(s)\right) ds = 1 \qquad (32)$$

The computed critical curve is presented in Figure 4.

Preprints (www.preprints.org) | NOT PEER-REVIEWED | Posted: 21 June 2022 doi:10.20944/preprints202206.0290.v1

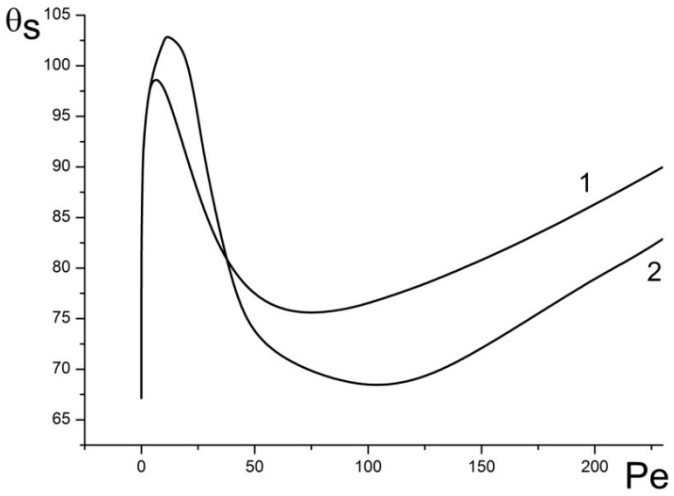

Figure 4. Critical curve $\theta_s = \theta_s(Pe)$. 1 – approximate model (29); 2 – original model (5); A=2.75x10^{-18}; Ar=0.012; h_s=7.14x10^2; g=1.0x10^{-20}; μ=91.67.

3.3 Analysis of the critical curve behaviour

Behaviour of critical curves and their dependence on parameters may be understood in more detail from Figures 5-9.

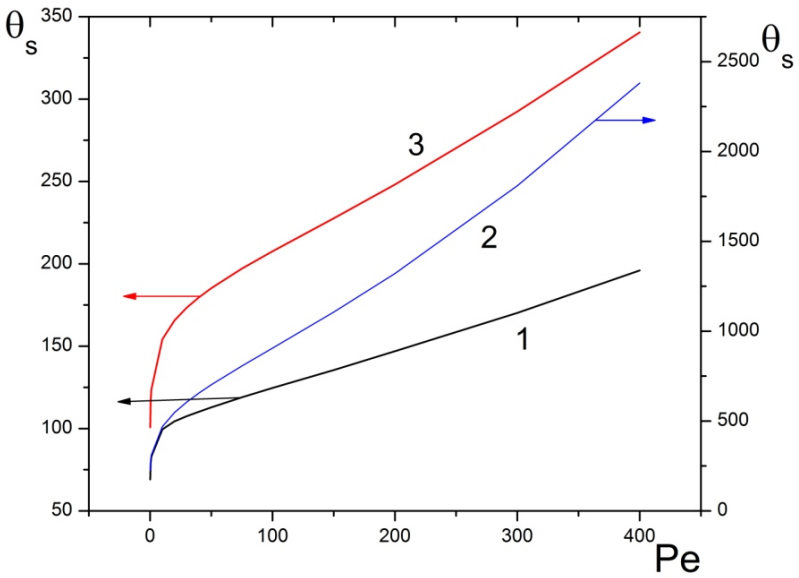

Figure 5. Monotonic critical curves. Approximate model (29). Ar=0.02; h_s=7.14x10^2; μ=75.0; 1 – A=2.75x10^{-13}; g=1.22 x10^{-15}; 2 – A=2.75x10^{-15}; g=1.22 x10^{-17}; 3 – A=2.75x10^{-18}; g=1.22 x10^{-20}.

Preprints (www.preprints.org) | NOT PEER-REVIEWED | Posted: 21 June 2022 doi:10.20944/preprints202206.0290.v1

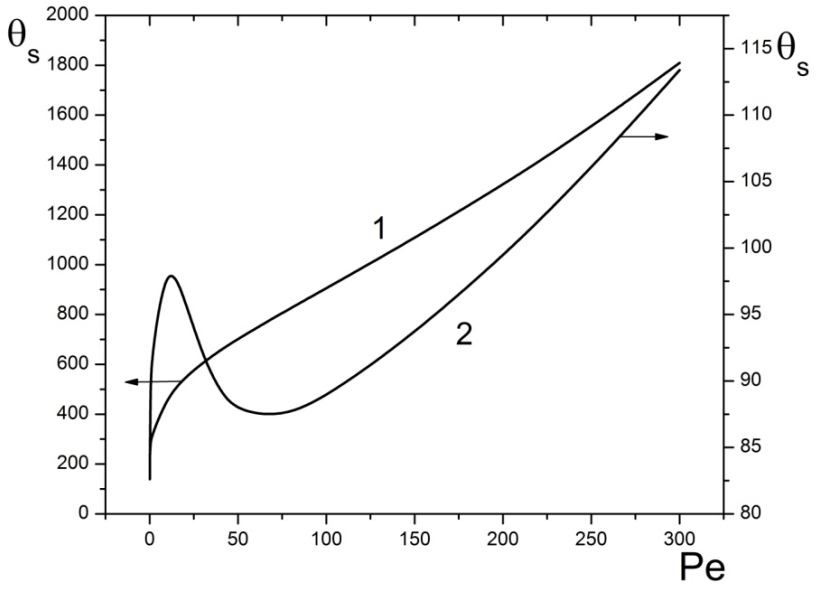

Figure 6. Transition from monotonic to non-monotonic critical curve. Approximate model (29). A=2.75x10^{-18}; h_s=7.14x10^2; μ=75.0; g=1.22 x10^{-20}; 1 – Ar=0.02; 2 – Ar=0.012.

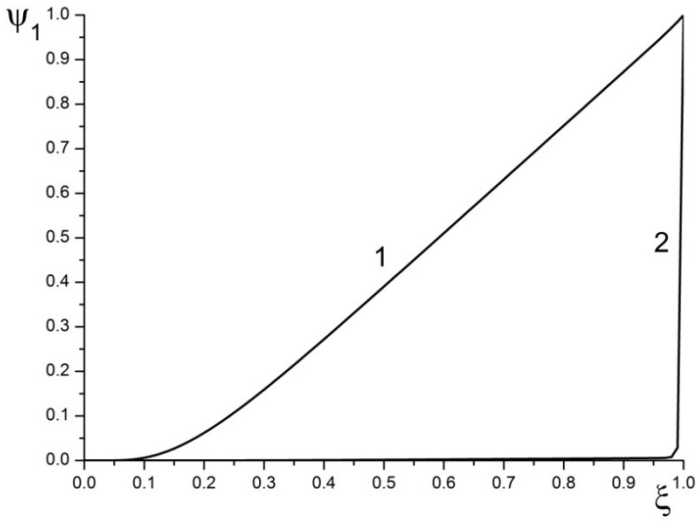

Figure 7. The integral $\Psi_1(\xi)$. Approximate model (29). A=2.75x10^{-18}; h_s=7.14x10^2; μ=75.0; g=1.22 x10^{-20}; 1 – monotonic critical curve. Ar=0.02; Pe=50.0; θ_s=702.01; 2 – non-monotonic critical curve. Ar=0.012; Pe=50.0; θ_s=87.70.

Preprints (www.preprints.org) | NOT PEER-REVIEWED | Posted: 21 June 2022 doi:10.20944/preprints202206.0290.v1

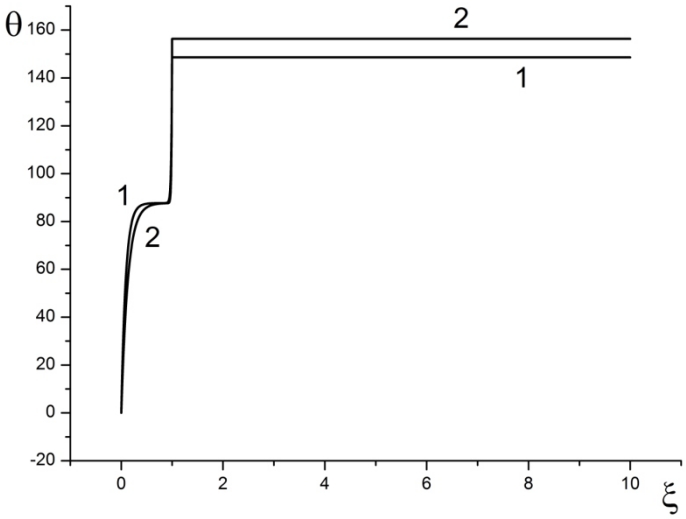

Figure 8 Solutions in the case of non-monotonic critical curve.

Approximate model (29).

A=2.75x10^{-18}; Ar=0.012; h_s=7.14x10^2; μ=75.0; g=1.22x10^{-20};

θ_s=87.70

1 – Pe=50.0

2 – Pe=84.35

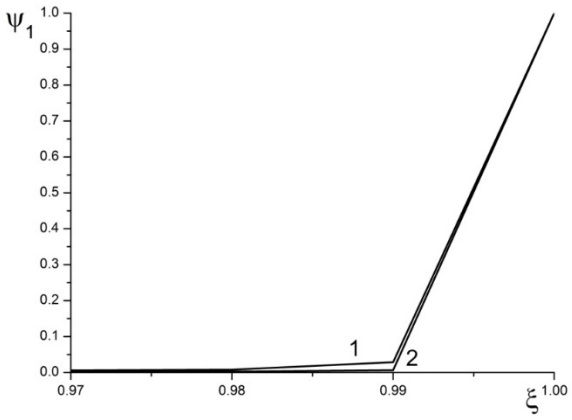

Figure 9 The integrals $\Psi_1(\xi)$ for the Figure 8 solutions.

Approximate model (29).

A=2.75x10^{-18}; Ar=0.012; h_s=7.14x10^2; μ=75.0; g=1.22 x10^{-20};

θ_s=87.70

1 – Pe=50.0

2 – Pe=84.35

Preprints (www.preprints.org) | NOT PEER-REVIEWED | Posted: 21 June 2022 doi:10.20944/preprints202206.0290.v1

It turns out that both monotonic and non-monotonic critical curves exist. The results presented in Figures 5 – 9 are obtained using the approximate model (29) with delta-function.

Figure 5 shows three curves drawn at different value of the parameters A and g. It is evident that all the three critical curves are monotonic.

Transition to non-monotonic behavior occurs upon variation of the Arrhenius number Ar (Figure 6), with all other parameters being kept constant. Non-monotonic behavior emerges upon decreasing Arrhenius number.

Particular type (monotonic or non-monotonic) of the critical curve is controlled by behavior of the integral

$$\Psi_1(\xi) = \frac{g}{Pe}\int_0^{\xi} f\left(\theta(s)\right)ds \qquad (33)$$

which must be equal to unity at $\xi = 1$.

Figure 7 demonstrates these integrals for monotonic and non-monotonic curves. For non-monotonic solution the total value of the integral accumulates in the small vicinity of the point $\xi = 1$.

In the non-monotonic case (curve 2, Figure 6) the same value of $\theta_s =$ 87.70 corresponds to the two values of the parameter Pe, namely $Pe =$ 50 and $Pe =$ 84.35.

The solutions $\theta(\xi)$ for these two values of Pe are presented in Figure 8, while Figure 9 presents the integrals $\Psi_1(\xi)$ for these solutions.

It is evident from Figure 9 that total values of the both integrals accumulate in the small vicinity of the point $\xi = 1$.

The critical curve decreases at the point ($Pe =$ 50, $\theta_s =$ 87.70), and increases at the point ($Pe =$ 84.35, $\theta_s =$ 87.70).

It may be concluded that sharp behaviour of the integral $\Psi_1(\xi)$ in the vicinity of the point $\xi = 1$ is the necessary condition for the critical curve to be non-monotonic.

Counterintuitive existence of non-monotonic critical curves may be explained in the following way.

Assuming the approximate δ - function model (29) and setting ξ_0=1 results in the following BVP for the temperature profile on $[0,1]$

$$\frac{d^2\theta}{d\xi^2} - Pe\frac{d\theta}{d\xi} + h_s\left(\theta_s - \theta\right) = 0 \qquad (34)$$

$$\theta(0) = 0; \quad \frac{d\theta}{d\xi}(1) = \mu \cdot Pe$$

and, for a given Pe the value of θ_s is determined from the condition

Preprints (www.preprints.org) | NOT PEER-REVIEWED | Posted: 21 June 2022 doi:10.20944/preprints202206.0290.v1

$$\frac{g}{Pe}\int_0^1 f\left(\theta(s)\right)ds = 1 \qquad (35)$$

where the source function $f\left(\theta\right)$ is given by the equation (5).

Let

$$\lambda_1 = \frac{Pe+\sqrt{Pe^2+4h_s}}{2};\quad \lambda_2 = -\frac{2h_s}{Pe+\sqrt{Pe^2+4h_s}} \qquad (36)$$

Then λ_1 is sufficiently large for $h_s = 720$, $Pe < 50$, while at the same time λ_2 is negative with sufficiently large absolute value, so that approximately

$$\theta(\xi) \approx \theta_s\left(1-\exp\left(\lambda_2\xi\right)\right)+\frac{\mu Pe}{\lambda_1}\exp\left(\lambda_1\left(\xi-1\right)\right) \qquad (37)$$

Let us consider the case where the value $\frac{g}{Pe}f\left(\theta_s\right)$ is negligibly small. It is only in this case when the original problem is well approximated by the model with δ - function source. In this case we can assume

$$\theta(\xi) = \theta_s + \frac{\mu Pe}{\lambda_1}\exp\left(\lambda_1\left(\xi-1\right)\right) \qquad (38)$$

and then

$$\frac{d\theta}{d\xi} = \lambda_1\left(\theta-\theta_s\right) \qquad (39)$$

We solve, under the above assumptions, the equation

$$F\left(\theta_s, Pe\right) = \frac{g}{Pe}\int_0^1 f\left(\theta(s)\right)ds = 1 \qquad (40)$$

with respect to θ_s at a fixed value of Pe.

It is easy to see that $F\left(\theta_s, Pe\right)$ is monotonic with respect to θ_s. Therefore, the solution $\theta_s\left(Pe\right)$ of the equation $F\left(\theta_s, Pe\right)=1$ is unique with respect to θ_s.

If $\frac{\partial F}{\partial Pe}>0$ at $F\left(\theta_s, Pe\right)=1$ then $\frac{d\theta_s}{dPe}<0$.

Let us calculate $\frac{\partial F}{\partial Pe}$.

Let $u=\theta-\theta_s$, then

Preprints (www.preprints.org) | NOT PEER-REVIEWED | Posted: 21 June 2022 doi:10.20944/preprints202206.0290.v1

$$F\left(\theta,Pe\right)=\frac{g}{Pe}\int_{1}^{\frac{\mu Pe}{\lambda_1}}\frac{f\left(\theta_s+u\right)}{\lambda_1 u}du \tag{41}$$

(We have assumed that the value $\frac{g}{Pe}f\left(\theta_s\right)$ is small and the lower bound of the integral is irrelevant).

Further,

$$\frac{\partial F}{\partial Pe}=\frac{2h_s}{\lambda_1^2\sqrt{Pe^2+4h_s}}\frac{\mu g}{Pe}\frac{f\left(\theta^*\right)}{\mu Pe}-$$

$$-\frac{2g}{Pe^3\sqrt{Pe^2+4h_s}}\int_{1}^{\frac{\mu Pe}{\lambda_1}}\frac{f\left(\theta_s+u\right)}{u}du=$$

$$=\frac{2h_s g f\left(\theta^*\right)}{\lambda_1^2 Pe^2\sqrt{Pe^2+4h_s}}-\frac{2\lambda_1}{Pe^2\sqrt{Pe^2+4h_s}} \tag{42}$$

Here $\theta^*=\theta(1)=\theta_s+\frac{\mu Pe}{\lambda_1}$, and we have used the fact that

$$\int_{1}^{\frac{\mu Pe}{\lambda_1}}\frac{f\left(\theta_s+u\right)}{u}du=\frac{\lambda_1 Pe}{g} \tag{43}$$

Therefore, under our assumptions, $\frac{d\theta_s}{dPe}<0$ if $f\left(\theta^*\right)>\frac{\lambda_1^3}{gh_s}$.

It is easy to see that upon increasing μ or decreasing Ar (at fixed g, Pe, h_s), $\theta_s\left(Pe\right)$ decreases, while $f\left(\theta^*\right)$ increases.

Therefore, by increasing μ or decreasing Ar, we can obtain points on the critical curve where $\frac{d\theta_s}{dPe}<0$.

3.4. Comparison with experimental data

Let us compare results of the present study with available experimental observations.Yakovlev *et al.* conducted a very detailed numerical investigation of flame stabilization process in thin-layered radial porous burner. It consisted of a mounting flange connected with a thin-layered porous shell. Flow configuration for the reported experiment may be considered as a flow through porous wall of the infinitely long hollow cylinder in the direction normal to the wall (i.e. in the plane perpendicular to the axial axis of symmetry of the cylinder). Flow direction is from the inner surface of the cylinder to the outer surface.

Within stable operating ranges, the flame front can be stabilized within the cavity of the burner (internal regime), within porous media (submerged flame) or above it (surface-stabilized flame), by adjusting equivalence ratio and the flow rate.

The first of these regimes (stabilization upstream from the lattice) is not considered in the present study, however, the latter two are of most interest. Similar to the present study, Yakovlev *et al.* observed two types of temperature distribution profiles, that is monotonic and non-monotonic. When flame stabilized within porous media (submerged regime), then non-monotonic profile was observed. When flame stabilized downstream from the surface (surface-stabilized regime), then monotonic profile was observed. This change of profile configuration upon flame front relocating from the porous to the gas region is quantitatively identical to the behavior reported in Figures 2 and 3 of the present study.

Mital *et al.* and Janvekar *et al.* considered porous burners of cylindrical shape, with the flow parallel to the to the axial axis of symmetry of the cylinder. This configuration would be asymptotically identical to the one used in the present study if the radius of the cylinder increases infinitely.

Both studies observed flame stabilization regime inside the porous material (submerged reaction zone) with non-monotonic temperature profiles similar the one presented in Figure 2.

Thus the studies of Yakovlev *et al.*, Mital *et al.* and Janvekar *et al.* provide indirect, but nevertheless very convincing support for the results of the present study.

4. Conclusions

Standing premixed combustion wave on a lattice burner has two qualitatively distinctive regimes: flame stabilizes either downstream from the burner surface, or inside the solid lattice.

For the first time, this fact has been proved absolutely rigorously using one-dimensional analytical model of reacting flow.

It has also been demonstrated using numerical simulations.

In the space of controlling parameters, the two stabilization regimes are separated by the specific dependence of the lattice temperature on the flow Peclet number (the critical curve), with all other parameters being fixed.

Transition from monotonic to non-monotonic regimes occurs as Arrhenius number sufficiently decreases.

Results of the present study agree qualitatively with available experimental data.

Funding information: No dedicated funding was available for the present study

Author contribution: All the authors contributed equally to the study.

Conflict of interest: The authors declare no conflict interest.

Abbreviations

BVP Boundary Value Problem

HTE Heat Transfer Equation

 doi:10.20944/preprints202206.0290.v1

LHS Left Hand Side

RHS Right Hand Side

Notation

Ascents

$\sim$ wave: dimensional, and only dimensional, variables

$\wedge$ cap: auxiliary non-dimensional variables

Latin

A	pre-exponential factor
Ar	Arrhenius number
C	reactant concentration
c_p	specific heat at constant pressure
E	activation energy
f	chemical source function
g	parameter
H	Heaviside function (unity for positive values of the argument; zero for non-positive values)
h	heat transfer coefficient
L	arbitrary large positive number
Pe	Peclet number
Q	heat of reaction
R	universal gas constant
S	lattice surface area per unit volume
T	temperature
u	gas mixture velocity
x	spatial coordinate
x_1	lattice thickness
Greek	
δ	delta-function
θ	temperature
κ	thermal diffusivity
λ	thermal conductivity
μ	parameter ($A/(3g)$)
ξ	spatial coordinate
ρ	density
τ	time
Subscripts	
s	surface
0	ambient; initial

Preprints (www.preprints.org) | NOT PEER-REVIEWED | Posted: 21 June 2022 doi:10.20944/preprints202206.0290.v1

APPENDIX A

Here an analytical solution for the approximate δ - function model (29) is presented. We solve the following problem

$$\frac{d^2\theta}{d\xi^2} - Pe\frac{d\theta}{d\xi} + \mu Pe\delta\left(\xi - \xi_0\right) + h\left(\theta_s - \theta\right) = 0 \qquad \text{(A.I)}$$

$$\theta(0) = 0 \qquad \frac{d\theta}{d\xi}(L) = 0 \qquad \xi \in (0, L)$$

The location ξ_0 is determined by the condition

$$\frac{g}{Pe}\int_0^{\xi_0} f\left(\theta(s)\right)ds = 1 \qquad \text{(A.II)}$$

The source function $f\left(\theta\right)$ is given by the eq. (5).

The parameters $\lambda_{1,2}$ used below are given by the eq. (36).

Let us solve the problem (A.I) at a fixed value of ξ_0.

Case 1. $0 \le \xi_0 < 1$

In this case solution has the form

$$\Theta_1\left(\xi, \xi_0\right) = \begin{cases} \theta_s\left(1 - \mathrm{e}^{\lambda_2\xi}\right) + C_{1,1}\left(\xi_0\right)\left(\mathrm{e}^{\lambda_1\xi} - \mathrm{e}^{\lambda_2\xi}\right); & \xi \in [0, \xi_0) \\ \theta_s + C_{3,1}\left(\xi_0\right)\left(\mathrm{e}^{\lambda_1\xi} - \dfrac{\lambda_1}{\lambda_2}e^{(\lambda_1-\lambda_2)}\mathrm{e}^{\lambda_2\xi}\right); & \xi \in (\xi_0, 1] \\ \theta_s + C_{3,1}\left(\xi_0\right)\left(\mathrm{e}^{\lambda_1} - \dfrac{\lambda_1}{\lambda_2}e^{(\lambda_1-\lambda_2)}\mathrm{e}^{\lambda_2}\right); & \xi \in (1, L] \end{cases} \qquad \text{(A.III)}$$

The matching conditions at $\xi = \xi_0$ are

Preprints (www.preprints.org) | NOT PEER-REVIEWED | Posted: 21 June 2022 doi:10.20944/preprints202206.0290.v1

$$\begin{cases} \theta_s\left(1-\mathrm{e}^{\lambda_2\xi_0}\right)+C_{1,1}\left(\mathrm{e}^{\lambda_1\xi_0}-\mathrm{e}^{\lambda_2\xi_0}\right)=\theta_s+C_{3,1}\left(\mathrm{e}^{\lambda_1\xi_0}-\dfrac{\lambda_1}{\lambda_2}e^{(\lambda_1-\lambda_2)}\,\mathrm{e}^{\lambda_2\xi_0}\right) \\ C_{3,1}\lambda_1\left(\mathrm{e}^{\lambda_1\xi_0}-e^{(\lambda_1-\lambda_2)}\,\mathrm{e}^{\lambda_2\xi_0}\right)+\theta_s\lambda_2\,\mathrm{e}^{\lambda_2\xi_0}-C_{1,1}\left(\lambda_1\,\mathrm{e}^{\lambda_1\xi_0}-\lambda_2\,\mathrm{e}^{\lambda_2\xi_0}\right)=-\mu Pe \end{cases} \quad \text{(A.IV)}$$

from where

$$C_{1,1}\left(\xi_0\right)=\frac{\theta_s\left(\lambda_1-\lambda_2\right)\lambda_2+\mu Pe\left(\mathrm{e}^{(\lambda_1-\lambda_2)}\,\mathrm{e}^{-\lambda_1\xi_0}\,\lambda_1-\mathrm{e}^{\lambda_2\xi_0}\,\lambda_2\right)}{\left(\lambda_1-\lambda_2\right)\left(\mathrm{e}^{(\lambda_1-\lambda_2)}\,\lambda_1-\lambda_2\right)} \quad \text{(A.V)}$$

$$C_{3,1}\left(\xi_0\right)=\frac{\lambda_2\left(\theta_s\left(\lambda_1-\lambda_2\right)+\mu Pe\left(\mathrm{e}^{-\lambda_1\xi_0}-\mathrm{e}^{\lambda_2\xi_0}\right)\right)}{\left(\lambda_1-\lambda_2\right)\left(\mathrm{e}^{(\lambda_1-\lambda_2)}\,\lambda_1-\lambda_2\right)}$$

Case 2. $\xi_0=1$

Solution has the form

$$\Theta_2\left(\xi,\xi_0\right)=\begin{cases} \theta_s\left(1-\mathrm{e}^{\lambda_2\xi}\right)+C_{1,2}\left(\xi_0\right)\left(\mathrm{e}^{\lambda_1\xi}-\mathrm{e}^{\lambda_2\xi}\right); & \xi\in[0,1] \\ C_{3,2}\left(\xi_0\right); & \xi\in(1,L] \end{cases} \quad \text{(A.VI)}$$

The matching conditions

$$\begin{cases} \theta_s\left(1-\mathrm{e}^{\lambda_2}\right)+C_{1,2}\left(\mathrm{e}^{\lambda_1}-\mathrm{e}^{\lambda_2}\right)=C_{3,2} \\ \theta_s\lambda_2\,\mathrm{e}^{\lambda_2}-C_{1,2}\left(\lambda_1\,\mathrm{e}^{\lambda_1}-\lambda_2\,\mathrm{e}^{\lambda_2}\right)=-\mu Pe \end{cases} \quad \text{(A.VII)}$$

 doi:10.20944/preprints202206.0290.v1

$$C_{1,2}\left(\xi_0\right)=\frac{\theta_s\lambda_2\,\mathrm{e}^{\lambda_2}+\mu Pe}{\left(\lambda_1\,\mathrm{e}^{\lambda_1}-\lambda_2\,\mathrm{e}^{\lambda_2}\right)} \qquad \text{(A.VIII)}$$

$$C_{3,2}\left(\xi_0\right)=\theta_s\left(1-\mathrm{e}^{\lambda_2}\right)+\frac{\left(\theta_s\lambda_2\,\mathrm{e}^{\lambda_2}+\mu Pe\right)}{\left(\lambda_1\,\mathrm{e}^{\lambda_1}-\lambda_2\,\mathrm{e}^{\lambda_2}\right)}\left(\mathrm{e}^{\lambda_1}-\mathrm{e}^{\lambda_2}\right)$$

Case 3. $\xi_0>1$

Solution has the form

$$\Theta_3\left(\xi,\xi_0\right)=\begin{cases}\theta_s\left(1-\mathrm{e}^{\lambda_2\xi}\right)+C_{1,3}\left(\xi_0\right)\left(\mathrm{e}^{\lambda_1\xi}-\mathrm{e}^{\lambda_2\xi}\right); & \xi\in[0,1]\\ C_{3,3}\left(\xi_0\right)+C_{4,3}\left(\xi_0\right)\mathrm{e}^{Pe\xi}; & \xi\in(1,\xi_0]\\ C_{3,3}\left(\xi_0\right)+C_{4,3}\left(\xi_0\right)\mathrm{e}^{Pe\xi_0}; & \xi\in(\xi_0,L]\end{cases} \qquad \text{(A.IX)}$$

Matching derivatives at $\xi=\xi_0$ gives

$$C_{4,3}\left(\xi_0\right)=\mu\,\mathrm{e}^{-Pe\xi_0} \qquad \text{(A.X)}$$

The matching conditions at $\xi=1$

$$\begin{cases}\theta_s\left(1-\mathrm{e}^{\lambda_2}\right)+C_{1,3}\left(\mathrm{e}^{\lambda_1}-\mathrm{e}^{\lambda_2}\right)=C_{3,3}+\mu\,\mathrm{e}^{Pe\left(1-\xi_0\right)}\\ -\theta_s\lambda_2\,\mathrm{e}^{\lambda_2}+C_{1,3}\left(\lambda_1\,\mathrm{e}^{\lambda_1}-\lambda_2\,\mathrm{e}^{\lambda_2}\right)=\mu Pe\,\mathrm{e}^{Pe\left(1-\xi_0\right)}\end{cases} \qquad \text{(A.XI)}$$

 doi:10.20944/preprints202206.0290.v1

$$C_{1,3}\left(\xi_0\right)=\frac{\theta_s\lambda_2\,\mathrm{e}^{\lambda_2}+\mu Pe\,\mathrm{e}^{Pe\left(1-\xi_0\right)}}{\left(\lambda_1\,\mathrm{e}^{\lambda_1}-\lambda_2\,\mathrm{e}^{\lambda_2}\right)} \qquad \text{(A.XII)}$$

$$C_{3,3}\left(\xi_0\right)=\theta_s\left(1-\mathrm{e}^{\lambda_2}\right)-\mu\,\mathrm{e}^{Pe\left(1-\xi_0\right)}+\frac{\left(\theta_s\lambda_2\,\mathrm{e}^{\lambda_2}+\mu Pe\,\mathrm{e}^{Pe\left(1-\xi_0\right)}\right)}{\left(\lambda_1\,\mathrm{e}^{\lambda_1}-\lambda_2\,\mathrm{e}^{\lambda_2}\right)}\left(\mathrm{e}^{\lambda_1}-\mathrm{e}^{\lambda_2}\right)$$

Solution of the BVP (A.I-A.II) on the whole interval $\left[0,L\right]$ is

$$\Theta\left(\xi,\xi_0\right)=\begin{cases}\Theta_1\left(\xi,\xi_0\right); & \xi_0\in\left[0,1\right)\\ \Theta_2\left(\xi,\xi_0\right); & \xi_0=1\\ \Theta_3\left(\xi,\xi_0\right); & \xi_0\in\left(1,L\right)\end{cases} \qquad \text{(A.XIII)}$$

References

1 Williams, F.A. (2018) Combustion Theory, CRC Press.

2 Kuo, K.K. (2005) Principles of Combustion, Wiley.

3 Zeldovich, Ya.B., Barenblatt, G.I., Librovich, V.B. and Makhviladze, G.M. (1980) Mathematical Theory of Combustion and Explosion, Nauka (In Russian).

4 Novozhilov, B.V. and Novozhilov, V.B. (2021) Theory of Solid-Propellant Nonsteady Combustion, Wiley-ASME Press.

5 Merzhanov, A.G. and Khaikin, B.I. (1992) Theory of Combustion Waves in Homogeneous Media, ISM RAS (In Russian).

6 Merzhanov, A.G. Self-propagating high-temperature synthesis: twenty years of search and findings. In: *Combustion and Plasma Synthesis of High-Temperature Materials*, Munir, Z.A., Holt, J.B. (Eds.), VCH, 1990, 1–53

7 Hirano, T. and Saito, K. (1994) Fire Spread Phenomena: The Role of Observation in Experiment, *Progress in Energy and Combustion Science*, 20(6), 461-485.

8 Fernandez-Pello, A.C. and Hirano, T. (1983) Controlling Mechanisms of Flame Spread, *Combustion Science and Technology*, 32(1-4), 1-31.

9 Smirnov, N.N. and Dimitrienko, I.D. (1992) Convective Combustion of Porous Compressible Propellants, *Combustion and Flame*, 89(3-4), 260-270.

10 Aldushin A.P., Matkowsky B.J., Schult D.A., Shkadinskaya G.V., Shkadinsky K.G., Volpert V.A. (1995) Porous medium combustion. In: Buckmaster J., Takeno T. (eds) Modeling in Combustion Science. Lecture Notes in Physics, vol 449. Springer, Berlin, Heidelberg. https://doi.org/10.1007/3-540-59224-5_25

11 Aldushin, A.P., Seplyarsky, B.S. (1978) Propagation of waves of exothermal reaction in porous medium during gas blow-through. Soviet Physics Doklady 23, 483–485.

12 Shkadinsky, K.G., Shkadinskaya, G.V., Matkowsky, B.J., Volpert, V.A.: Two front traveling waves in filtration combustion, SIAM J. Appl. Math. **53** (1993) 128–140.

13 Schult, D.A., Matkowsky, B.J., Volpert, V.A. and Fernandez-Pello, A.C. (1995) Propagation and Extinction of Forced Opposed Flow Smolder Waves. Comb. and Flame, 101(4), 471-490.

14 Wahle, C.W. and Matkowsky, B.J. (2001) Rapid, Upward Buoyant Filtration Combustion Waves Driven by Convection, Combustion and Flame, 124, 14-34.

15 Yakovlev, I., Maznoy, A. and Zambalov, S. (2021) Pore-scale Study of Complex Flame Stabilization Phenomena in Thin-layered Radial Porous Burner, Combustion and Flame, 231, 111468.

16 Sangjukta, D., Sahoo, N. and Muthukumar, P. (2020) Experimental Studies on Biogas Combustion in a Novel Double Layer Inert Porous Radiant Burner, Renewable Energy, 149, 1040-1052.

17 Mital, R., Gore, J. P. and R. Viskanta (1997) A Study of the Structure of Submerged Reaction Zone in Porous Ceramic Radiant Burners, Combustion and Flame, 111, 175-184.

18 Fursenko, R., Maznoy, A., Odintsov, E., Kirdyashkin, A., Minaev, S. and Sudarshan, K. (2016) Temperature and Radiative Characteristics of Cylindrical Porous Ni–Al Burners, International Journal of Heat and Mass Transfer, 98, 277–284.

19 Ferguson, J. C., Sobhani, S. and Ihme, M. (2021) Pore-resolved Pimulations of porous Media Combustion with Conjugate Heat Transfer, Proceedings of the Combustion Institute, 38, 2127–2134.

20 Bedoya, C., Dinkov, I., Habisreuther, Zarzalis, P. N., Bockhorn, H. and Parthasarathy, P. (2015) Experimental study, 1D Volume-averaged Calculations and 3D Direct Pore Level Simulations of the Flame Stabilization in Porous Inert Media at Elevated Pressure, Combustion and Flame, 162, 3740–3754.

21 Sirotkin, F., Fursenko, R., Kumar, S. and Minaev, S. (2017) Flame Anchoring Regime of Filtrational Gas Combustion: Theory and Experiment, Proceedings of the Combustion Institute, 36, 4383–4389.

22 Yakovlev, I. and Zambalov, S. (2019) Three-dimensional Pore-scale Numerical Simulation of Methane-air Combustion in Inert Porous Media under the Conditions of Upstream and Downstream Combustion Wave Propagation through the Media, Combustion and Flame, 209, 74–98.

23 Billerot, , P.-L., Dufresne, L. , Lemaire, R. and Seers, P. (2020) 3D CFD Analysis of a Diamond Lattice-based Porous Burner, Energy, 207, 118-160.

24 Wood, S. and Harris, A. T. (2008) Porous Burners for Lean-burn Applications, Progress in Energy and Combustion Science, 34, 667– 684.

25 Wua, C.-Y., Chen, K.-H. and Yang, S. Y. (2014) Experimental Study of Porous Metal Burners for Domestic Stove Applications, Energy Conversion and Management, 77, 380–388.

26 Dehaj, M. S., Ebrahimi, R., Shams, M. and Farzaneh, M. (2017) Experimental Analysis of Natural Gas Combustion in a Porous Burner, Experimental Thermal and Fluid Science, 84, 134–143.

27 Janvekar, A. A., Miskam, M.A., Abas, A., Ahmad, Z. A., Juntakan, T. and Abdullah, M.Z. (2017) Effects of the Preheat Layer Thickness on Surface/Submerged Flame, During Porous Media Combustion of Micro Burner, Energy, 122, 103-110.

28 Gao, H.B., Qu, Z.G., Feng, X.B. and Tao, W.Q. (2014) Methane/Air Premixed Combustion in a Two-layer Porous Burner with Different Foam Materials, Fuel, 115, 154–161.

29 Al-attab, K.A., Ho, J. C. and Zainal, Z.A. (2015) Experimental Investigation of Submerged Flame in Packed Bed Porous, Media Burner Fueled by Low Heating Value Producer Gas, Experimental Thermal and Fluid Science, 62, 1–8.

30 Arutyunov, V.S., Belyaev, A.A., Lidskii, B.V., Nikitin, A.V., Posvyanskii, V.S. and Shmelev, V,M. (2018) Numerical Solution of the Problem of Surface Combustion on Flat Porous Matrix, AIP Conf. Proc. 2046, 020075; https://doi.org/10.1063/1.5081595.

 doi:10.20944/preprints202206.0290.v1

31 Incropera, F.P. and DeWitt, D.P. (2002) Fundamentals of Heat and Mass Transfer, Wiley.

32 Borman, G.L. and Ragland, K.W. (1998) Combustion Technology, McGraw-Hill.